Supplementary Information

Aptamer single-molecule dispersion on single-atom anchoring sites for high-selectivity *in vivo* detection

Jing Huang, Shiting Gu, Xue Zhou, Yibin Liu, Zhonghai Zhang*

School of Chemistry and Molecular Engineering, East China Normal University, Shanghai 200241, China

E-mail: zhzhang@chem.ecnu.edu.cn

Experimental section

Chemicals and materials. A 0.1 mm thick titanium foil (99.6%, Jinnia Metal, China) was cut into pieces of 40×10 mm^2. Ethylene glycol (EG), ammonia fluoride (NH_4F), potassium chloride (KCl), sodium chloride (NaCl), potassium dihydrogen phosphate (KH_2PO_4), sodium phosphate (Na_2HPO_4), chloroauric acid ($HAuCl_4$), 6-mercapto-1-hexanol (MCH), dopamine (DA), norepinephrine (NE), epinephrine (EP), serotonin hydrochloride (5-HT), levodopa (L-DOPA), 3,4-Dihydroxyphenylacetic acid (DOPAC), carbidopa, tyrosine (Tyr), glutamate (Glu), γ-aminobutyric acid (GABA), arachidonic acid (AA), acetylcholine (ACh), nomifensine maleate salt, α-methyl-DL-tyrosine methyl ester hydrochloride (αMPT), 1-methyl-4-phenyl-1, 2, 3, 6 -tetrahydropyridine (MPTP) were purchased from Macklin Chemical and used as received. All aqueous solutions were prepared using deionized water (DI) with a resistivity of 18.2 MΩ cm at 25 °C. All oligonucleotide sequences used for the present study were synthesized and purified by Sangon Biotech, Shanghai, China. Oligonucleotide sequences used in this study is published from previous study (Science 362, 319–324 (2018)).

Strand	Sequence (5'→3')	Concentration
DA Aptamer	GGA CGA CGC CAG TTT GAA GGT TCG TTC GCA GGT GTG GAG TGA CGT CGT CC/3SH C6/	2 uM
Sensor	/56-FAM/ GGA CGA CGC CAG TTT GAA GGT TCG TTC GCA GGT GTG GAG TGA CGT CGT CC/3SH C6/	50 nM
Capture	CGT CGT CCC GAG AG/3Dab/	20 nM

Materials characterization. The morphologies of samples were characterized by scanning electron microscopy (SEM, Gemini450, Zeiss), The low magnification TEM images and EDS mapping were acquired at 200 kV using a JEM-2100F JEOL equipped with an X-ray energy dispersive spectrometer (EDS: X-Max 80T, Oxford, UK) for chemical composition analyses. For atomic resolution imaging, the measurements were performed on an aberration-corrected high-angle annular dark field scanning transmission electron microscopy (AC HAADF-STEM, JEOL Grand ARM300). EDS mapping images were taken under HAADF-STEM mode. The chemical compositions and status were analyzed by X-ray photoelectron spectroscopy (XPS) with an Axis Ultra instrument (Kratos Analytical) under ultrahigh vacuum (< 10^{-8} Torr) using a monochromatic Al Kα X-ray source. The electrochemical measurements were performed on CHI 660E electrochemical working station. The photocurrent was measured under the illumination of NIR light (infrared ray lamp bulb with wavelength centered at 760 nm with intensity of 30 mW cm^{-2}). Kd constant was measured by Microplate Reader (infinite M200 pro). Raman spectra were measured through DXR Raman Microscope (ThermoFisher). The content of Au in the sample was determined on inductively couple plasma optical emission spectrometer (ICP-OES, Thermo Fisher, iCAP7200). The diffuse reflectance UV-Vis-NIR adsorption spectra (DRS) was detected on a spectrophotometer (Shimadzu, UV 2600).

Preparation of TiO_2 nanotube photoelectrode. The pristine TiO_2 nanotube photoelectrodes were synthesized using a two-step anodization process. Prior to the anodization process, the Ti foils underwent degreasing by sonicating in ethanol and DI

water, followed by drying in a pure nitrogen stream. The anodization process employed a conventional two-electrode system with the Ti foil serving as the anode and a Pt foil serving as the cathode, respectively. The electrolytes used consisted of 0.32 wt% NH4F in EG solution with 2.7 vol% DI water. All anodization steps were performed at an ice bath temperature. During the first anodization process, the Ti foils were anodized at 60 V for 30 min, and the as-grown nanotubes with a regular arrangement were subsequently removed from the Ti foil substrate by ultrasonication in DI water. The same Ti foil with patterned nanocaves then underwent the second anodization sequentially at 30 V for 30 min to adjust the size of the nanocaves. After the two-step anodization, the prepared TiO_2 samples were cleaned with DI water and dried with nitrogen gas. Then, the prepared TiO_2 nanoconcaves based photonic crystal were annealed in air at 500 °C for 1 h with a heating rate of 5 °C/min. The as-anodized TiO_2 photoelectrodes were sealed in a glass tube in vacuum condition. Finally, the as-sealed glass was annealed at temperature of 500 ℃ for 1 h to fabricate TiO_2 nanotube photoelectrodes with defects.

Fabrication of Au SA/TiO_2 and Au NP/TiO_2. A dilute sulfuric acid solution (0.5 M) was used to prepare the Au precursor, by adding $HAuCl_4$. The as-prepared TiO_2 photoelectrodes were immersed in 50 mL of the Au precursor for 1 h. Next, a typical two-electrode system was set up with Ti foil as the working electrode and Pt foil as the counter electrode, and Au precursor and TiO_2 were completely immersed in liquid nitrogen for about 5 minutes. The frozen mixture was then slowly electrochemically reduced at -10 V potentials. After reduction, the frozen electrolyte was melted at room

temperature, and the prepared Au SA/TiO_2 was washed with DI water and dried with nitrogen gas. The Au NP/TiO_2 were deposited with Au nanoparticles (Au NPs) in a sputtering process, in which the size of Au NPs and surface defects amplification degree can be regulated through manipulation of the sputtering time.

Procedure of the fabrication of PEC aptasensors. The Au SA/TiO_2 and Au NP/TiO_2 photoelectrodes were modified with the aptamer by the way of incubation, and the aptamers related to Au through Au–S bonds. To ensure the full incubation and ensure the strength of the Au–S bond, the mixture was gently shaken for 16 h, followed by thoroughly rinsing with deionized water to remove the unbonded aptamers. After that, the photoelectrode was also incubated with 1 mM MCH for about 1 h to screen the nonspecific combination sites.

PEC performance of photoelectrodes and aptasensors. The PEC characterizations of the aptamer/Au SA/TiO_2 and aptamer/Au NP/TiO_2 were evaluated with a three-electrode system, which used the followings as working electrodes and Pt foil, Ag/AgCl as counter electrode, and reference electrodes, respectively. The photoelectrochemical biosensing potential used here was optimized to be 0 V (vs SCE) under the illumination of NIR light. The electrolytes were implanted in artificial cerebrospinal fluid (aCSF).

Preparation of Au nanoparticles.

Measurement of dissociation constant (K_d). An aptamer/competitor strategy was employed. For measurement of Kd_1, firstly, 8 different concentrations of quencher (capture) solution in RNase/DNase-free water were prepared. And then, the sensor solution was mixed with the quencher strand. The mixture was incubated for 5 minutes

in a hot water bath (95 ℃) and cooled slowly to the room temperature in the dark. Transferred appropriate amount of solution into a well in the plate next. Finally, read on a fluorescence plate reader (ex/em = 485 nm / 535 nm). Following this, the same method was used to measure K_{d2}. The K_d values of Au NPs were measured by the same process.

Fabrication of the gold nanoparticles. The preparation method is adopted by a typical way in Nat Protoc 1, 246–252 (2006). Firstly, synthesize aqua regia and immerse the 200 mL two-neck flask, magnetic stir bar, stopper, and condenser in it for 15 minutes and rinse with deionized and Millipore-filtered water to ensure a contamination-free synthesis environment. Then, fill the two-neck flask with 98 mL of Millipore water and add 2 mL of 50 mM $HAuCl_4$ to achieve a final concentration of 1 mM $HAuCl_4$. After that, attach the condenser, place the stopper, and set the flask to reflux on a hot plate with continuous stirring. Once refluxing begins, remove the stopper, add 10 mL of 38.8 mM sodium citrate, and replace the stopper, noting the color change to deep red, then continue refluxing for 20 minutes. Finally, turn off the heat and let the system cool to room temperature under stirring. The nanoparticles should be approximately 13 nm in diameter, with an extinction value of about 2.4 at the 520-nm plasmon peak and a concentration of about 13 nM.

Density functional theory (DFT) calculations. All the calculations were carried out based on density functional theory (DFT) implemented in DS-PAW software. The electron-ion interactions were described by the projector augmented wave (PAW) method and the exchange correlation energy was described within Perdew-Burke-

Ernzerhof (PBE) functional in the generalized gradient approximation (GGA). The anatase TiO_2 (101) surface is modeled with a periodically repeated slab. To avoid the interaction between two layers, a 15 Å vacuum layer was added at the top of surface. Only the top layer was relaxed during the optimization, and the bottom layer was fixed as the bulk layer. The surface optimization was done with an energy cutoff of 400 eV with a k-mesh of 3×3×1, and an energy and force convergence of 1×10^{-5} eV and 0.02 eV/Å respectively. Van der Waals (vdW) interaction was taken into account at the DFT-D2 level as proposed by Grimme. It is known that the DFT method had the incomplete self-interaction cancellation for transition metal. Thus, to mitigate such localization deficiency, the DFT+U approach (U=2 eV) were employed for Ti atoms and Au atoms. The adsorption of molecules on the surfaces was computed under the same setting as mentioned before in the optimization of the bare surfaces. The adsorption energy of the molecules on the surfaces were calculated as:

$E_{abs}=E_{molecule@slab}-E_{slab}-E_{molecule}$

Atomic charges were calculated from electronic structure by Bader charge analysis. Differential charges were used to study the electron transfer.

Modification of antifouling hydrogel layer. The antifouling interface of hydrogel was prepared by using diethylacrylamide and hydroxyethylacrylamide as mixed acrylamide hydrogel monomers. Hydrogel preploymer containing 20 wt% arylamide monomer, 1 wt% lithium phenyl-2,4,6-trimethylbenzoylphosphinate (LAP) as photoinitator, and 1 wt% methylenebisacrylamide were dissolved into DI water. The prefabricated hydrogel mixture was coated on the surface of aptamer/Au SA/TiO_2, and crosslinked under UV

light to obtain Gel/aptamer/Au SA/TiO_2 photoelectrode.

In vivo PEC performance.

Animals. All procedures involving animals were conducted with the approval of the Animal Ethics Committee in ECNU, China. Male C57 mice (6-8 weeks old, weight ranges from 18 to 20 g) were purchased from Shanghai SLAC Laboratory animal Co. Ltd. And all surgical procedures for mice were conducted in accordance with the Guidelines for the Care and use of Laboratory Animals of ECNU. The mice were housed with adequate food and water in an environment with suitable temperature and humidity and under a 12 h light/dark schedule with adequate food and water.

MPTP-induced mouse model of Parkinson's disease (PD). The procedure of model surgery was made referring of previous report (Metab Brain Dis (2010) 25:177–183, Nat. Protoc. 2, 141–151 (2007), Handbook of Neurotoxicity. Cham: Springer International Publishing, 1-41 (2021)). The experimental mouse of PD was induced by MPTP (20 mg/kg) via intraperitoneal every 2 hours for four times a day, and after 90 minutes DA became minimum levels. The mice in the control group were injected with the same volume of normal saline.

Aptamer/Au SA/TiO_2 for in vivo DA sensing in striatum. C57 mice were anesthetized by an isoflurane gas anesthesia machine and wrapped in a heating pad to maintain the body temperature at 37 °C. The mice were placed in a stereotaxic frame (Beijing Tide-Gene Biotechnology Development Centre) with the incisor bar set at 5 mm above the interaural line and appropriately placed holes were drilled through the skull. The micro-photoelectrode was implanted in mice brain of the right striatum (AP = 0.72 mm, L=

2.5 mm anterior to bregma, and V=5.0 mm from the surface of skull). Then the PEC in vivo detection of DA was performed in a two-electrode model of Aptamer/Au SA/TiO_2 and Pt wire without external potentials. As the electrode was immediately implanted, the photocurrent response can be regarded as the baseline without DA absorption. After few seconds (4.7 s in Fig. S 30), the DA reached a stable adsorption equilibrium on the surface of electrodes, the DA concentrations were detected under illumination of NIR light. PEC measurements were performed using a CHI 660e electrochemical workstation (Shanghai CH instrument Co., China) to monitor the levels of dopamine before and after the i.p. injection of nomifensine (20mg/kg), α-methyl-DL-tyrosine methyl ester hydrochloride (αMPT, 250mg/kg) and K^+(80 mM). Photocurrent signal acquisition was performed again 30 minutes after drug injection.

Aptamer/Au SA/TiO_2 for multiple brain regions monitoring. The anesthetic PD mice was fixed on the stereotaxic frame. According to standard stereotaxic procedures, the photoelectrodes were implanted into different mice brain areas and affixed to the skull using dental cement. The coordinates of prefrontal cortex (PFC), hippocampus (Hip), striatum (Str) is (AP = +2.5 mm, ML = -0.6 mm, DV = -2.0 mm), (AP = -2.0 mm, ML = -1.5 mm, DV = -1.0 mm) and (AP = +0.6 mm, ML = -2.0 mm, DV = -3.0 mm), respectively. After measuring for ten minutes, L-DOPA was used to increase DA concentration. The photocurrent was recorded for continuous 60 minutes for both normal and PD mice.

In Vivo and In Vitro Data Calibration Methods: Cingulum (AP = -1.1 mm, ML = -0.8 mm, DV = - 1.4 mm), a brain region with hardly no dopamine, was chosen as the

reference of *in vivo* and *in vitro* environment. Each working electrodes was measured basic photocurrent constant in vitro. And the constants before injecting L-DOPA were represented as *in vivo* constants. The ratio between the two of cingulum was regarded as the difference between in vivo and in vitro environment. Consequently, according to the ratio, it was easily to confirm the photocurrent changes caused by DA in vivo in the other three brain regions.

Open field test. The locomotor abilities of mice in different groups were measured using the open field test. Mice were allowed to adapt to the environment for two hours prior to testing. They were then placed to individually the same wall of a 50 × 50 × 30 cm white square box for 5 min monitoring by camera. The movements and trajectories of the mice were analyzed by software (Supermaze, Shanghai Xinruan soft Information Technology Co., LTD).

New object recognition (NOR) test. All behavioral experiments were conducted in late afternoon/early evening dim light. Before the commencement of the behavioral testing, each mouse was habituated to a rectangular case. In each sample phase, mice were allowed to explore two copies of the same object for a total 3 min. The test trial was given after 1 h. The discrimination ratio was calculated as the difference in time spent by each animal exploring the object from habituated object compared with the object from new object divided by the total time spent exploring both objects in the first minute of the test period.

The temporal order recognition (TOR) task. The temporal order recognition (TOR) task was performed as previously described. Before the commencement of the

behavioral testing, each mouse was habituated to a rectangular case. In each sample phase, mice were allowed to explore two copies of the same object for a total 3 min. The exploration for sample 1 and sample 2 were 1 h interval. The test trial was given 4 h after sample phase 2. All behavioral experiments were conducted in late afternoon/early evening dim light. If temporal order memory is intact, the mice will spend more time exploring the novel object (i.e., sample 1 presented less recently), rather than the familiar object (i.e., sample 2 presented more recently). The discrimination ratio was calculated as the difference in time spent by each animal exploring the object from sample 1 compared with the object from sample phase 2 divided by the total time spent exploring both objects in the first minute of the test period.

Immunocytochemistry and immunofluorescence staining. The normal and the PD mice were killed by the method of cervical dislocation and then removed the brain. The fresh brain tissues were immediately put into 0.1 M PB containing 4% paraformaldehyde (vol/vol) for 24 h at room temperature. Then take the tissue into the embedding frame and dehydrate leached wax. After that, the wax-soaked tissue was embedded and sectioned. Then the immunohistochemistry and immunofluorescence were performed following a classical procedure. Firstly, brain sections were rinsed with Triton X-100 in TBS for 5 min for three times. Subsequently, brain sections were blocked with 10% (wt/vol) goat serum and 1% (wt/vol) in TBS at room temperature for 2 h, and gently shake off, incubated with secondary antibody (anti-TH rabbit polyclonal antibody (1:1000)) at 4 ℃ for 12 h and rinsed thrice with Triton X-100 in TBS for 5

min. Finally, brain sections were mounted with the commercial antifade medium containing DAPI. The FL images were captured on a high-resolution confocal FL microscope.

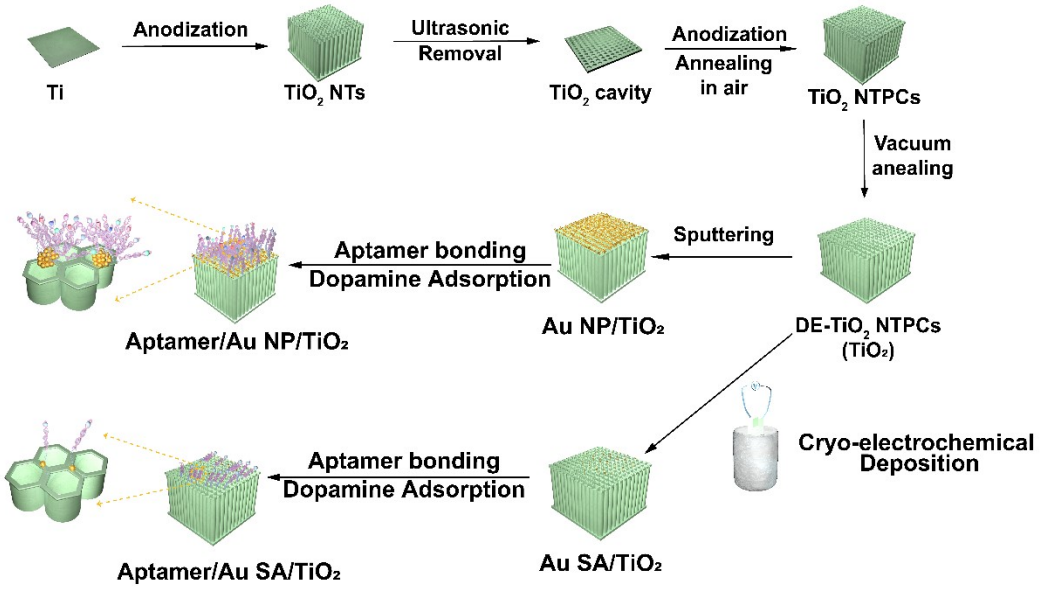

Fig. S1 Schematic illustration of fabrication of aptamer/Au SA/TiO_2 and aptamer/Au NP/TiO_2.

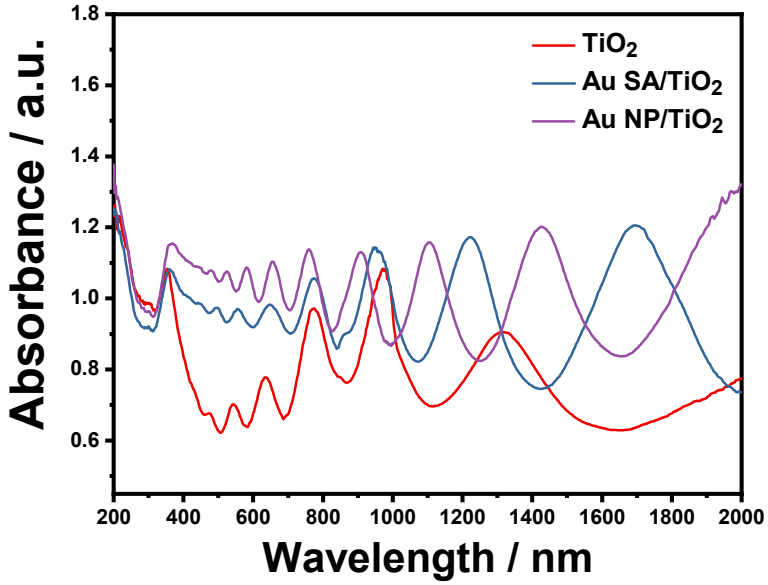

Fig. S2 The diffuse reflectance UV-vis-NIR adsorption spectrum of TiO_2, Au SA/TiO_2 and Au NP/TiO_2.

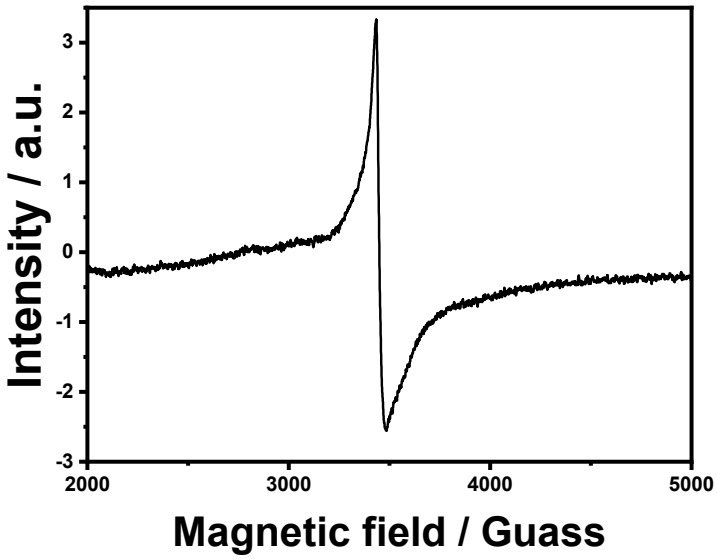

Fig. S3 EPR spectrum of TiO_2.

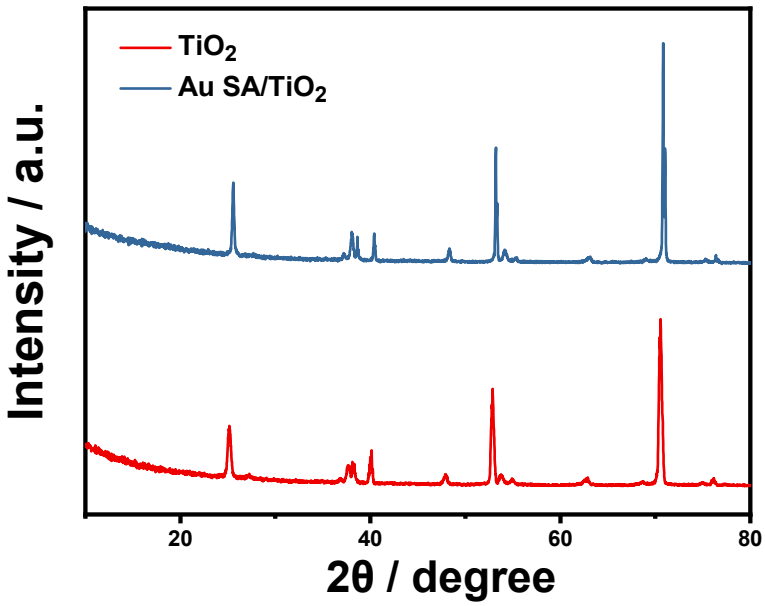

Fig. S4 X-ray diffraction (XRD) spectrums of TiO_2 and Au SA/TiO_2.

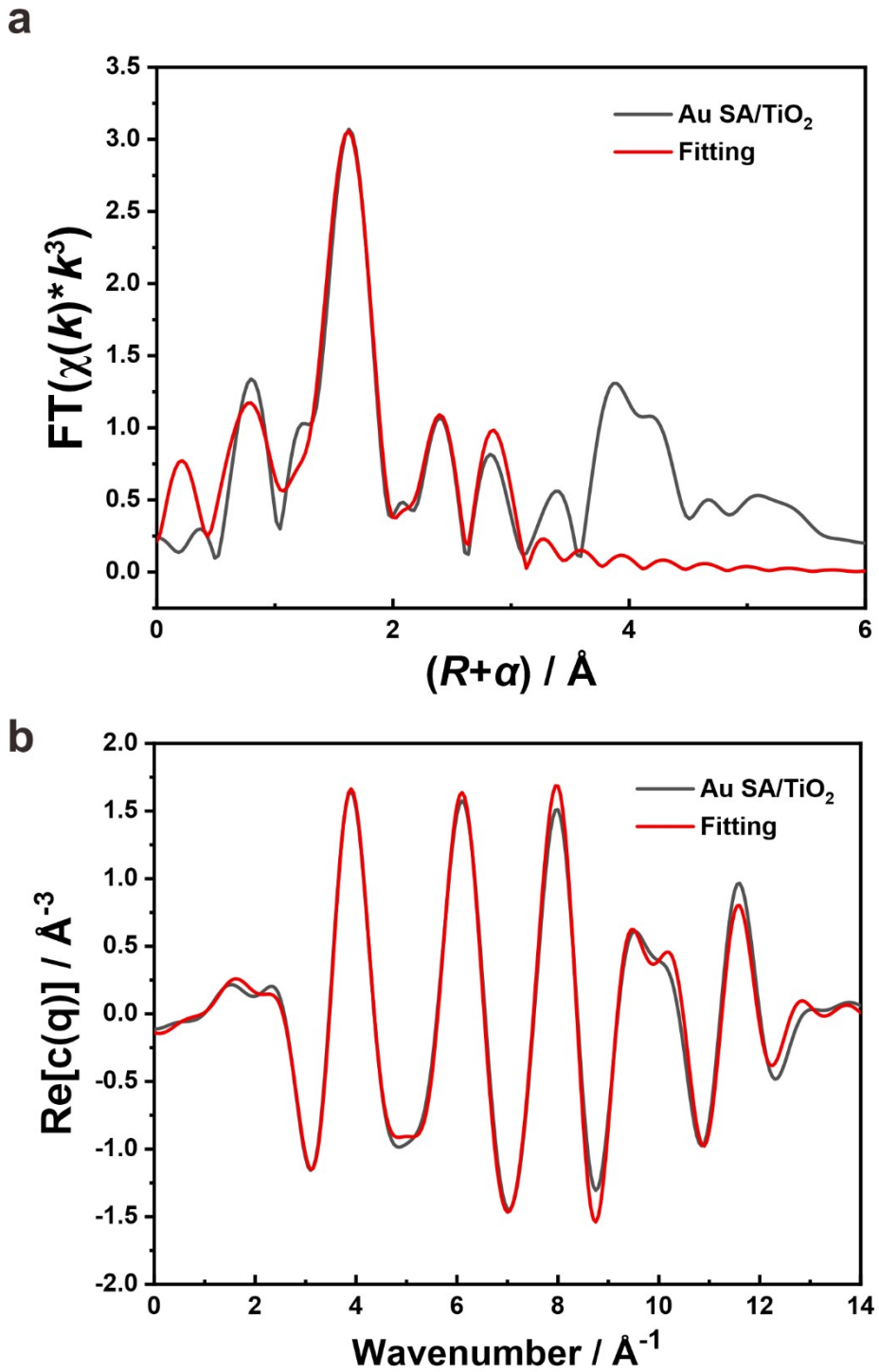

Fig. S5 The corresponding EXAFS r space (a) and inverse FT (b) fitting curves of Au SA/TiO_2.

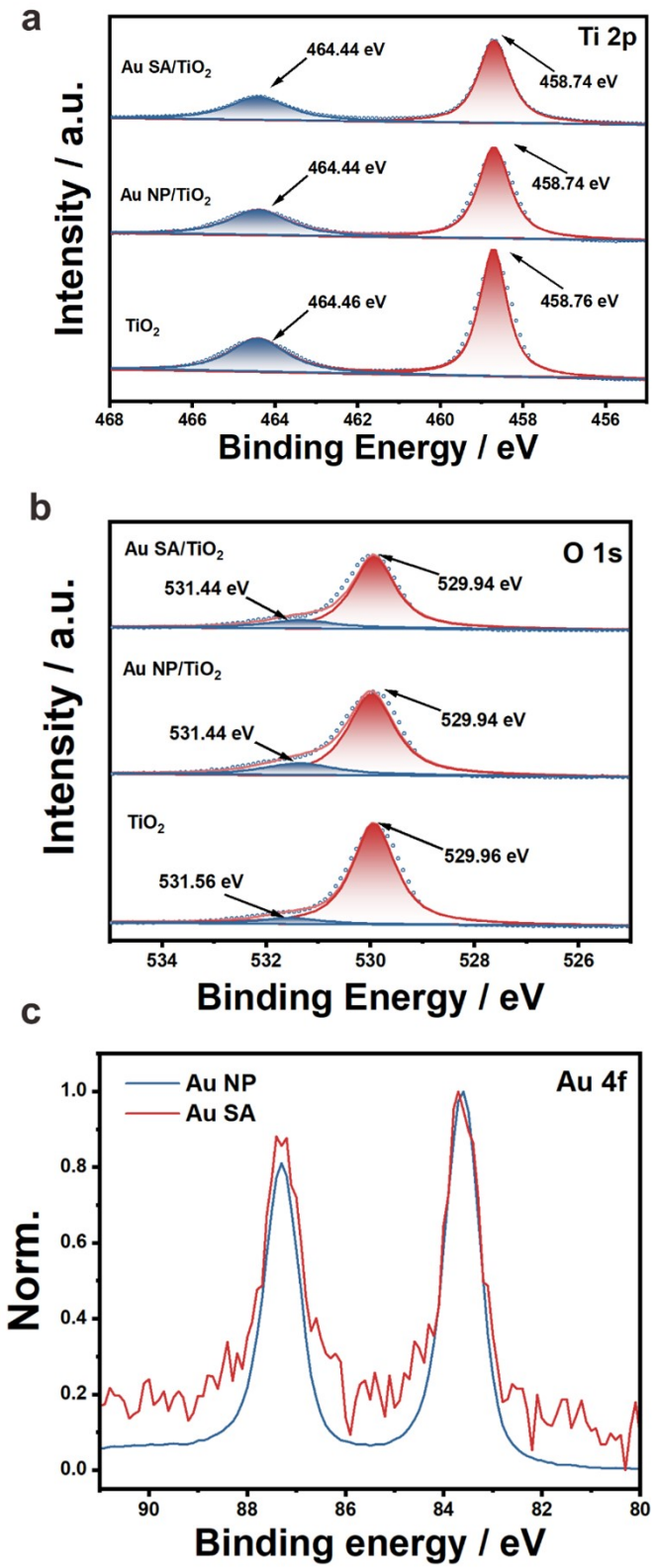

Fig. S6 TiO_2, Au NP/TiO_2, Au SA/TiO_2 core-level XPS (a) Ti 2p (b) O 1s, and (c) Au 4f.

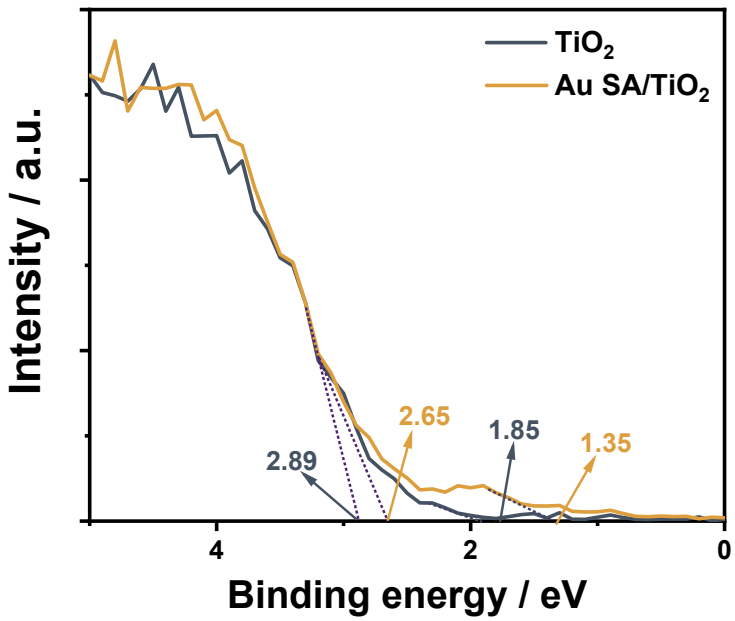

Fig. S7 XPS of valence band of TiO_2 and Au SA/TiO_2.

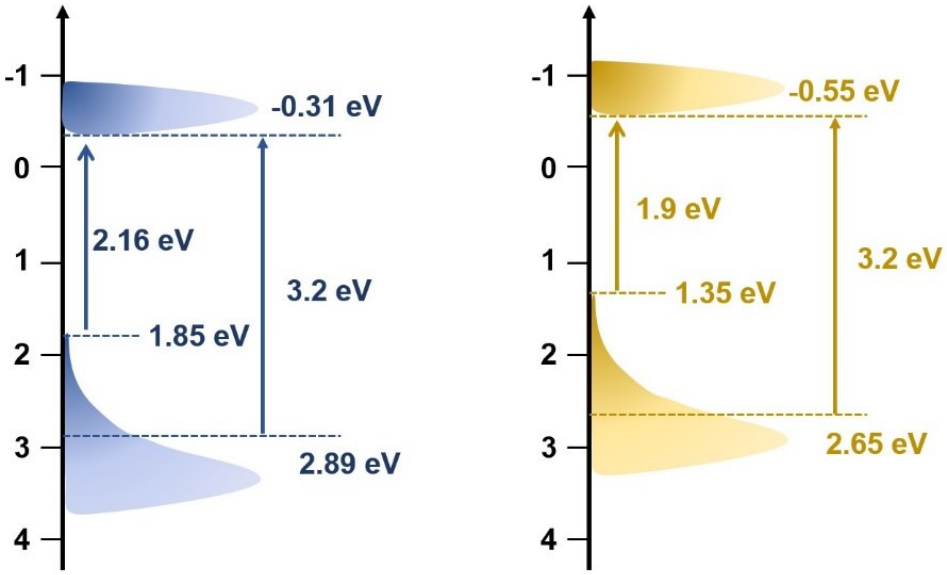

Fig. S8 Schematic diagram of band energy levels of TiO_2 (left) and Au SA/TiO_2 (right).

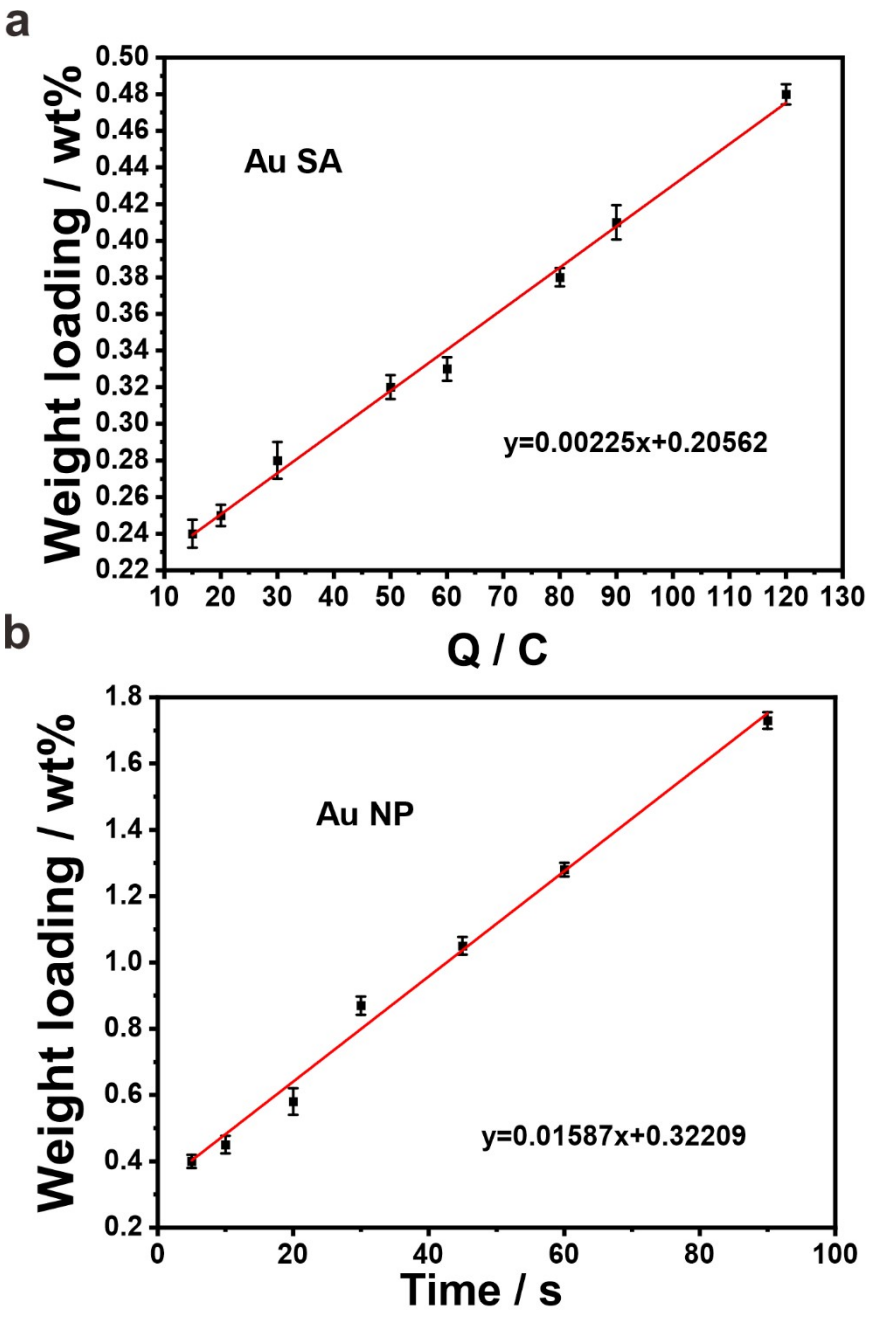

Fig. S9 Au content measured by inductively coupled plasma-atomic emission spectrometry (ICP-AES) versus the amount of charge accumulated during cryo-electrochemical deposition of Au SA (a) and the time of sputtering process of Au NP (b).

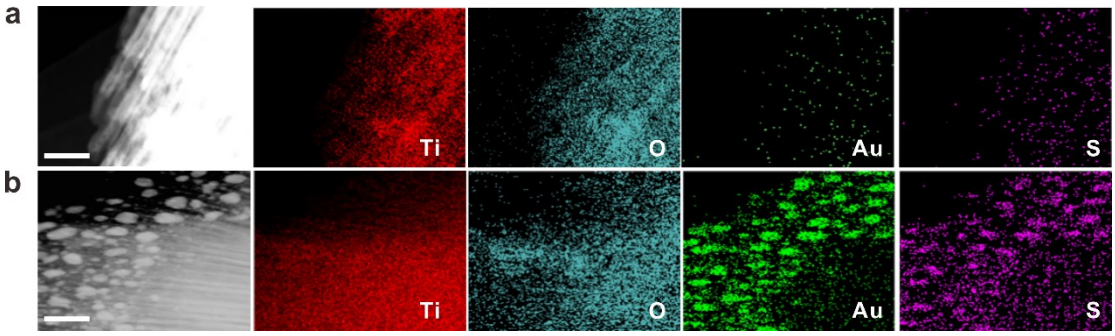

Fig. S10 HADDF-STEM image of aptamer/Au SA/TiO_2 and the responding EDS elemental mapping images of Ti, O, Au, S, the scale bar is 500 nm; (b) HADDF-STEM image of aptamer/Au NP/TiO_2 and the responding EDS elemental mapping images of Ti, O, Au, S, the scale bar is 500 nm.

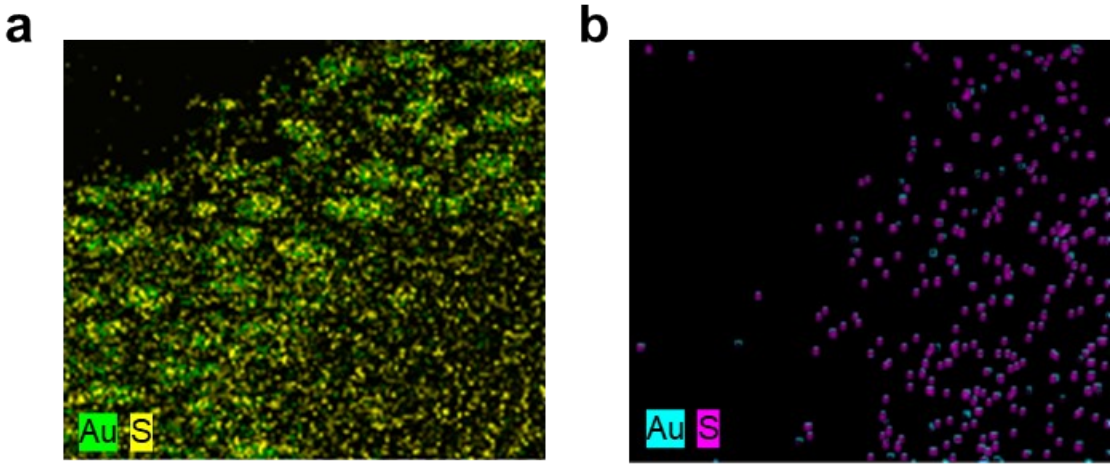

Fig. S11 EDS elemental mapping images of merging Au and S channels of (a) aptamer/Au NP/TiO_2 and (b) aptamer/Au SA/TiO_2.

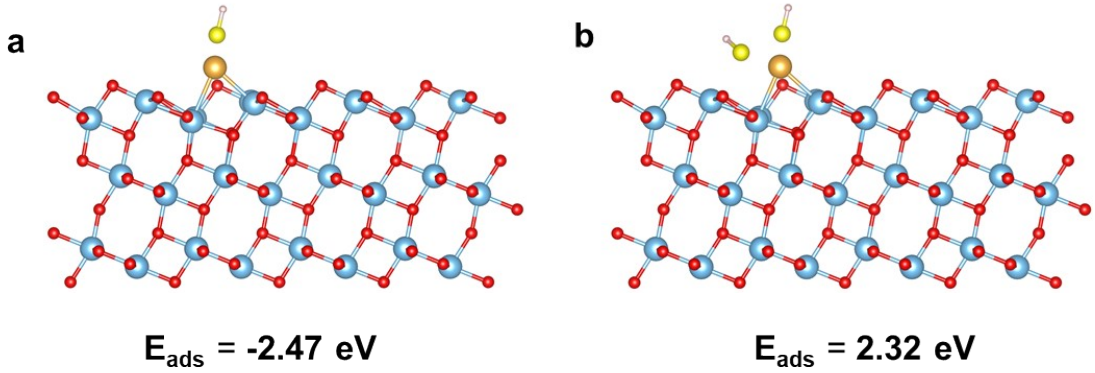

Fig. S12 DFT calculations of adsorption energy of (a) one thiol group on Au SA/TiO_2 and (b) two thiol groups on Au SA/TiO_2.

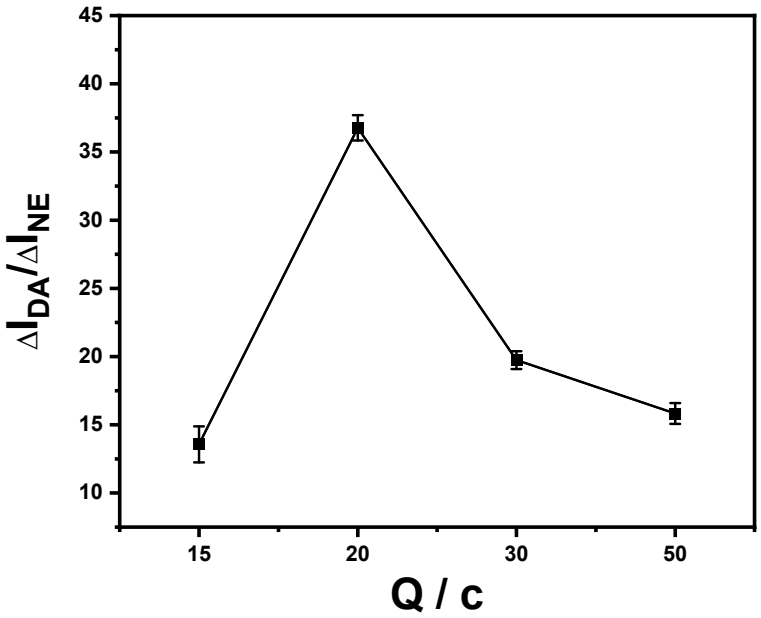

Fig. S13 Photocurrent response ratios of DA/NE of aptamer/Au SA/TiO_2 with different Au single atom contents.

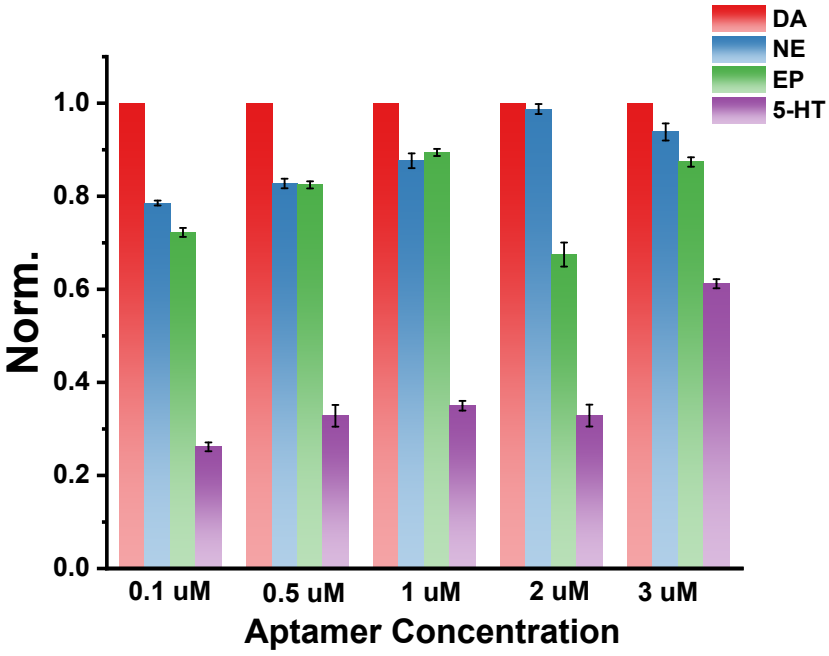

Fig. S14 Selectivity study of aptamer/Au NP/TiO_2 with different concentration of aptamer.

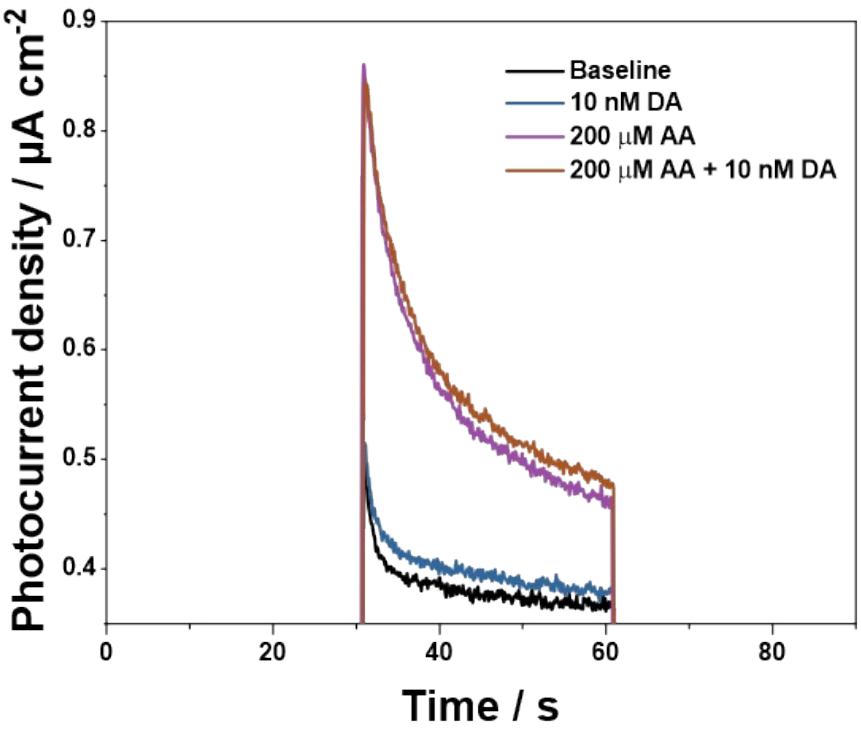

Fig. S15 Photocurrent density response of 10 nM DA on aptamer/Au SA/TiO_2 with/without 200 μM AA.

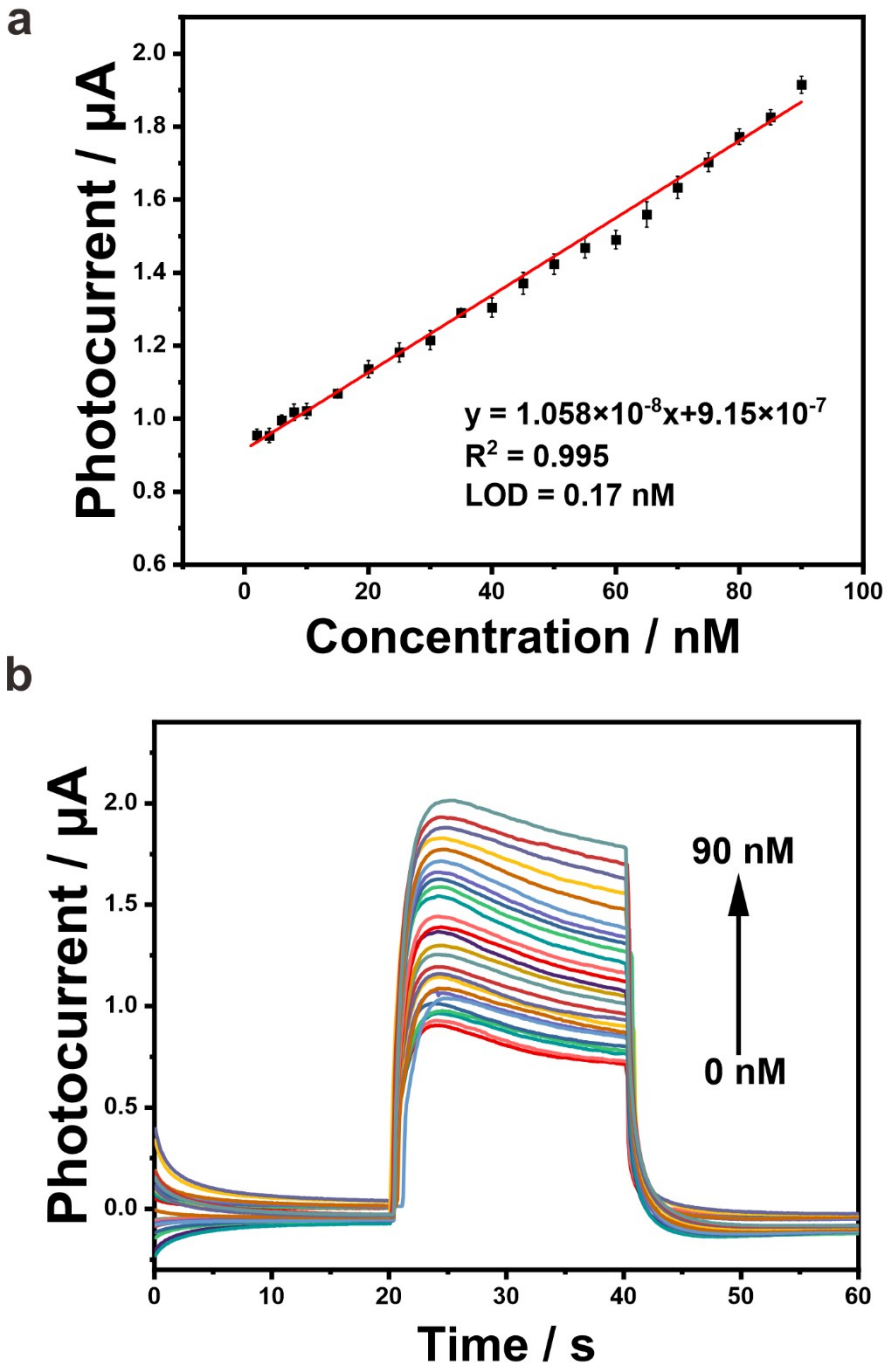

Fig. S16 Aptamer/Au SA/TiO_2 PEC plots (a) and its linear calibration curve (b) in aCSF.

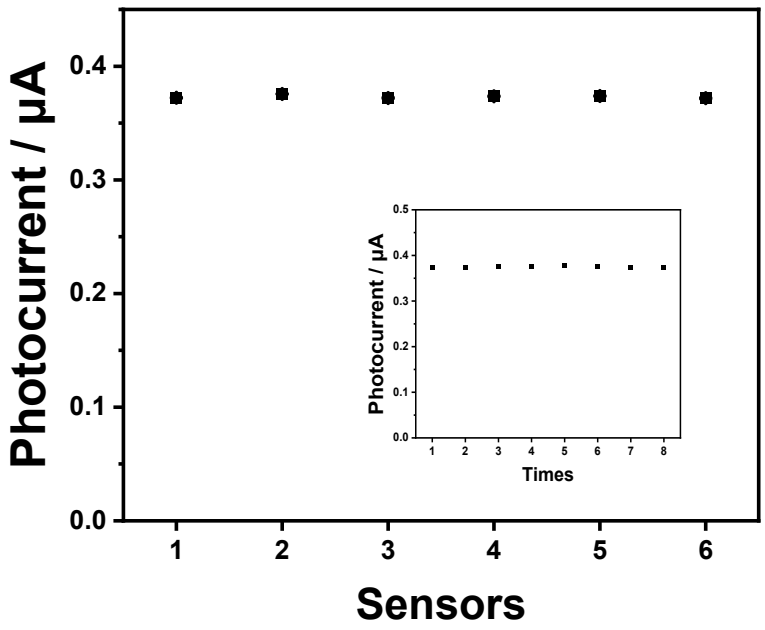

Fig. S17 Reproducibility and repeatability of aptamer/Au SA/TiO_2.

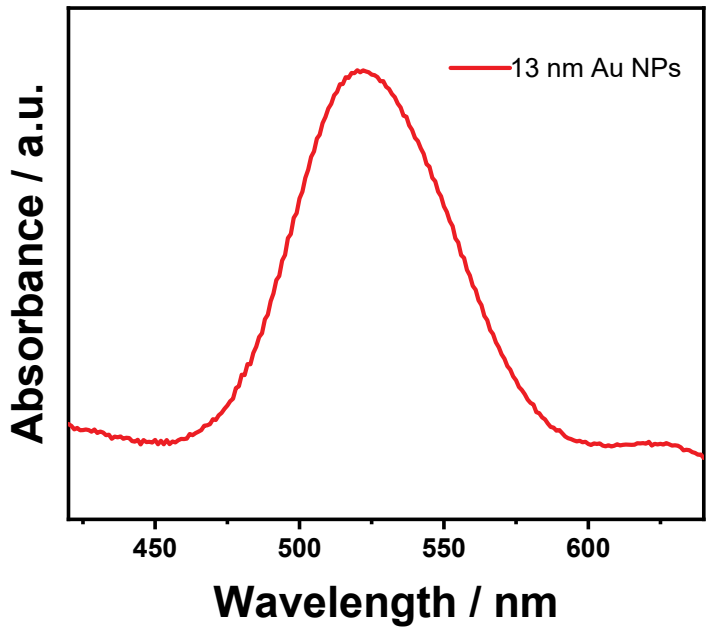

Fig. S18 UV-visible spectra of Au nanoparticles with the peak of about 521 nm.

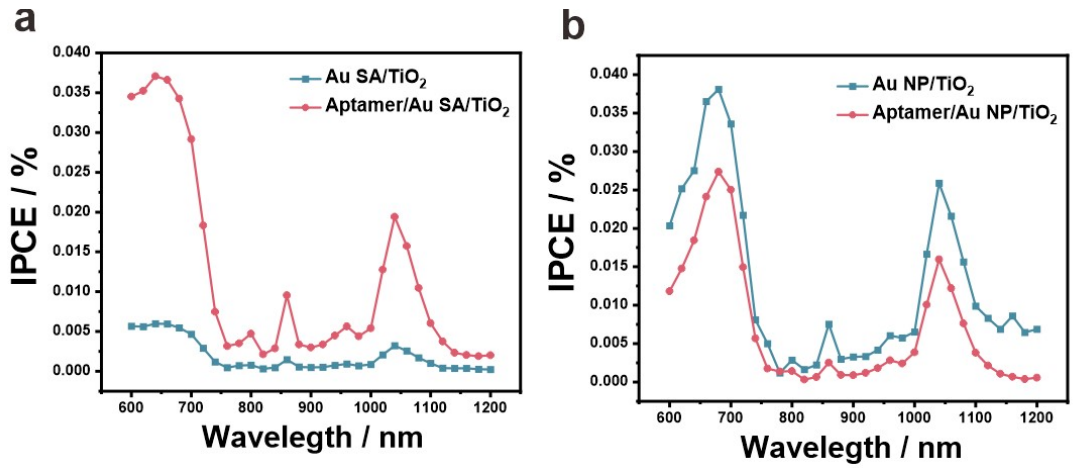

Fig. S19 IPCE plots of Au SA/TiO_2 (a) and aptamer/Au SA/TiO_2 with DA (a) and Au NP/TiO_2 and Aptamer/Au NP/TiO_2 (b).

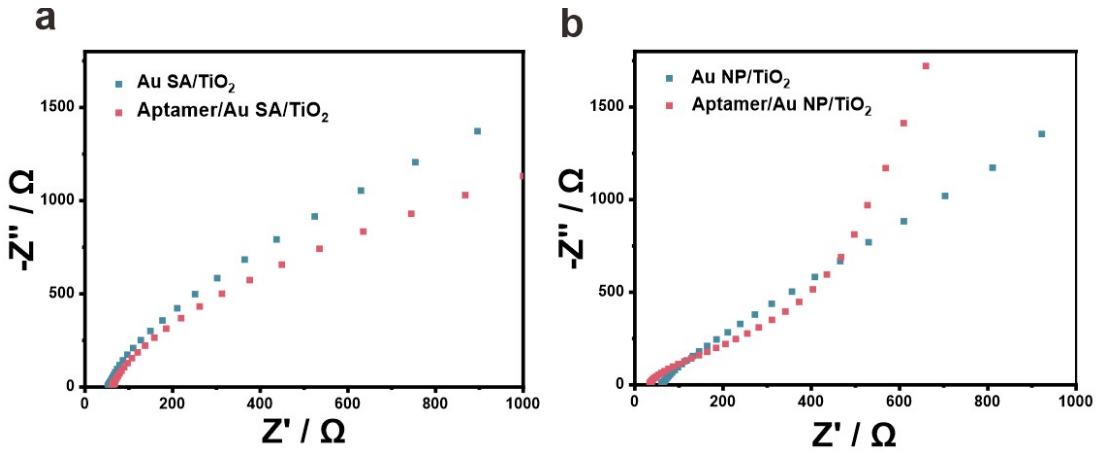

Fig. S20 Electrochemical impedance spectra (EIS) of Nyquist plots of Au SA/TiO_2 and aptamer/Au SA/TiO_2 (a) and Au NP/TiO_2 and aptamer/Au NP/TiO_2 (b).

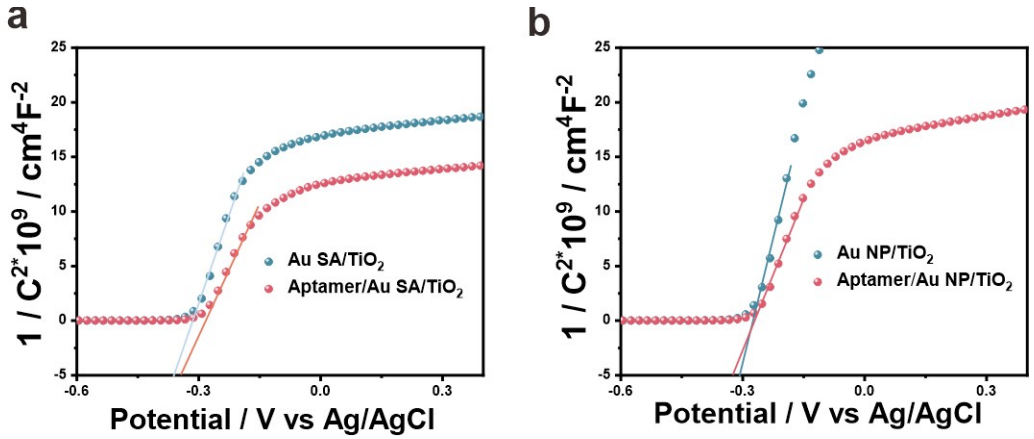

Fig. S21 Mott−Schottky plots of Au SA/TiO_2 and aptamer/Au SA/DE-TiO_2 (a) and Au NP/TiO_2 and aptamer/Au NP/TiO_2 (b).

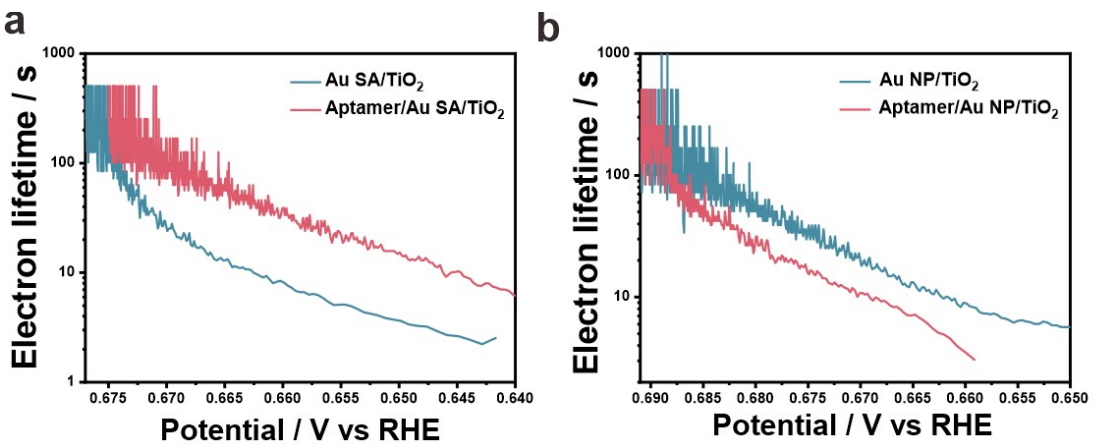

Fig. S22 Electron lifetime curves of Au SA/TiO_2 and aptamer/Au SA/TiO_2 (a) and Au NP/TiO_2 and Aptamer/Au NP/TiO_2 (b).

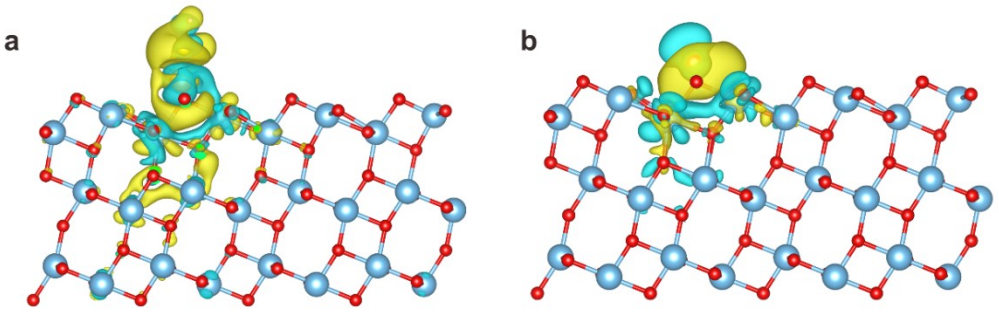

Fig. S23 DFT calculations of local charge density difference of Au SA/TiO_2 (a) and -SH linkage to Au SA/TiO_2 (b).

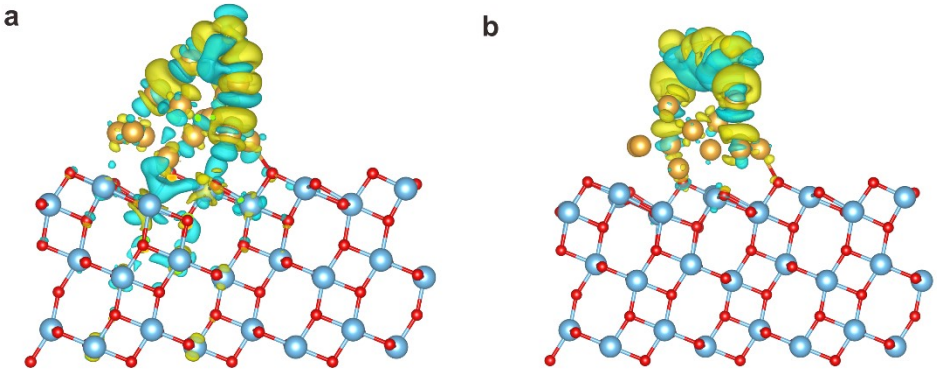

Fig. S24 DFT calculations of local charge difference of Au NP/TiO_2 with one thiol bond (a) and Au NP/TiO_2 with two thiol bonds (b).

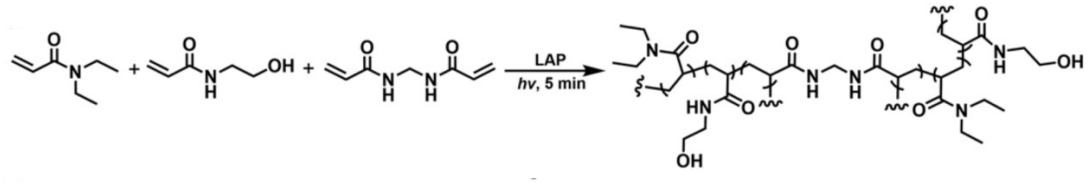

Fig. S25 Polyacrylamide hydrogel (λ = 350nm) was photopolymerized with phenyl-2,4,6-trimethylbenzoyl lithium hypophosphite (LAP) as free radical photoinitiator.

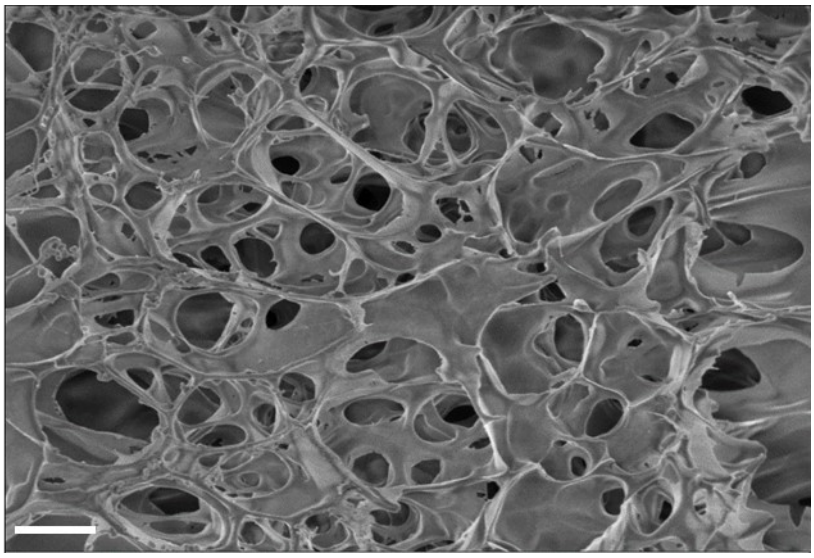

Fig. S26 SEM images of Gel. The scale bar is 2 μm.

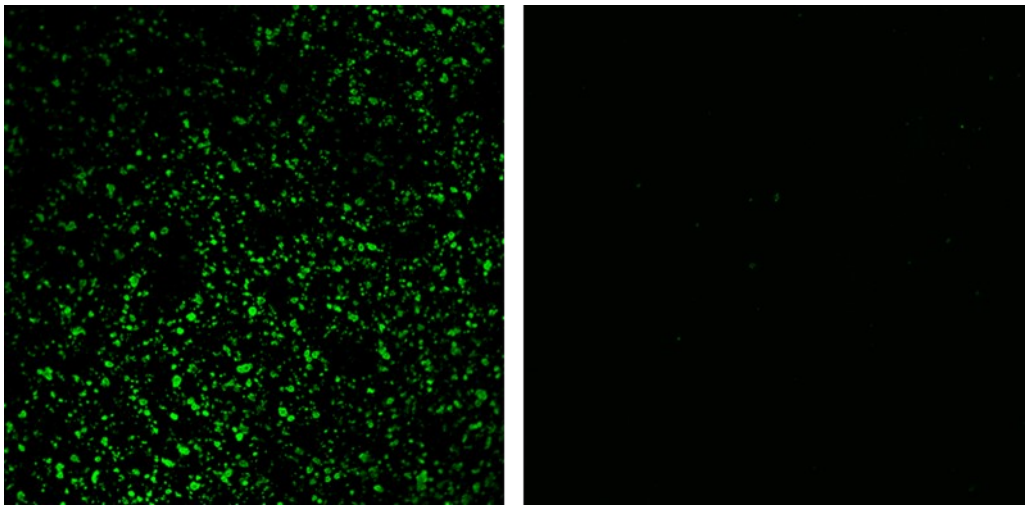

Fig. S27 Confocal laser scanning microscope images of (left) aptamer/Au SA/TiO_2 and (right) Gel/Aptamer/Au SA/TiO_2 electrode after immersing in aCSF containing 20 mg/mL albumin from bovine serum (BSA).

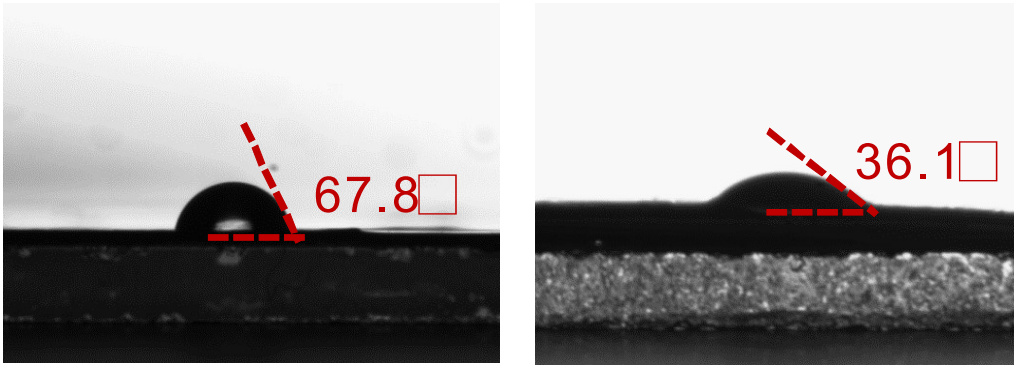

Fig. S28 Static water contact angle on Aptamer/Au SA/TiO_2 (left) and Gel/Aptamer/Au SA/TiO_2 (right) electrode.

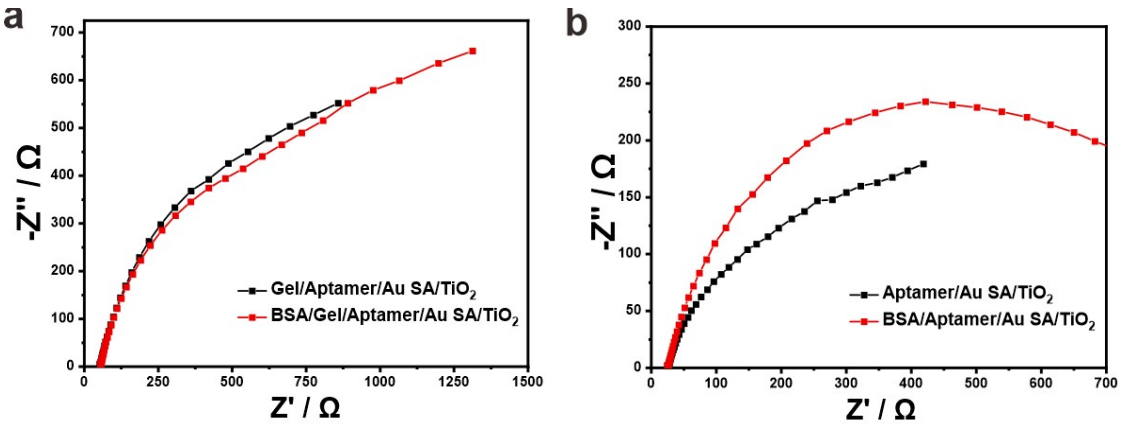

Fig. S29 Impedance responses of Gel/Aptamer/Au SA/TiO_2 (a) and Aptamer/Au SA/TiO_2 (b) electrode after immersing in aCSF containing 20 mg/mL BSA.

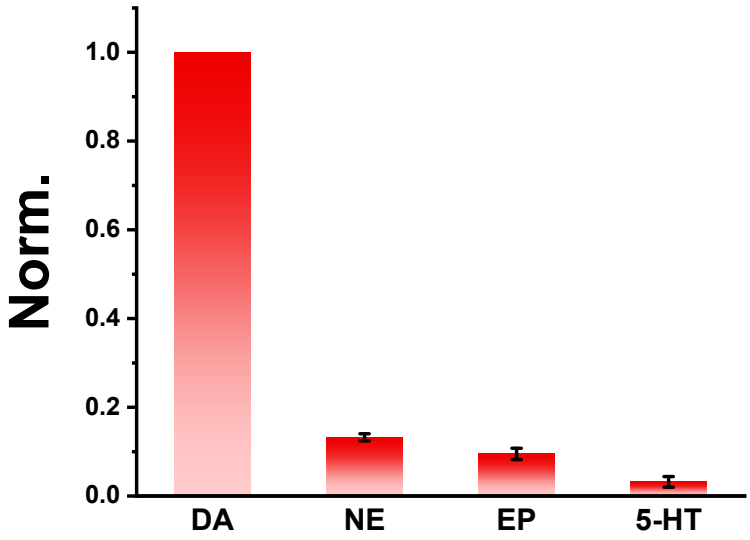

Fig. S30 Selectivity of DA on Gel/aptamer/Au SA/TiO_2 with interferences of NE, EP and 5-HT.

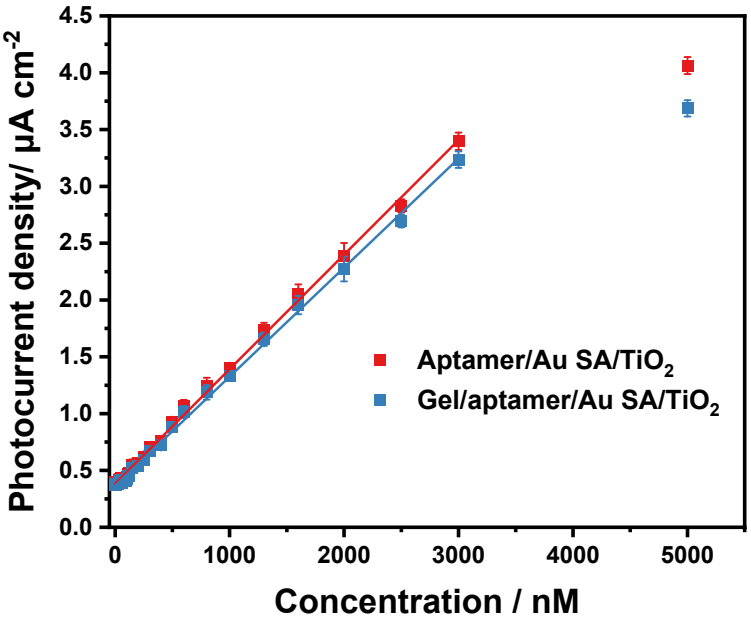

Fig. S31 Linear calibration curve of Gel/aptamer/Au SA/TiO_2 and the comparison of aptamer/Au SA/TiO_2.

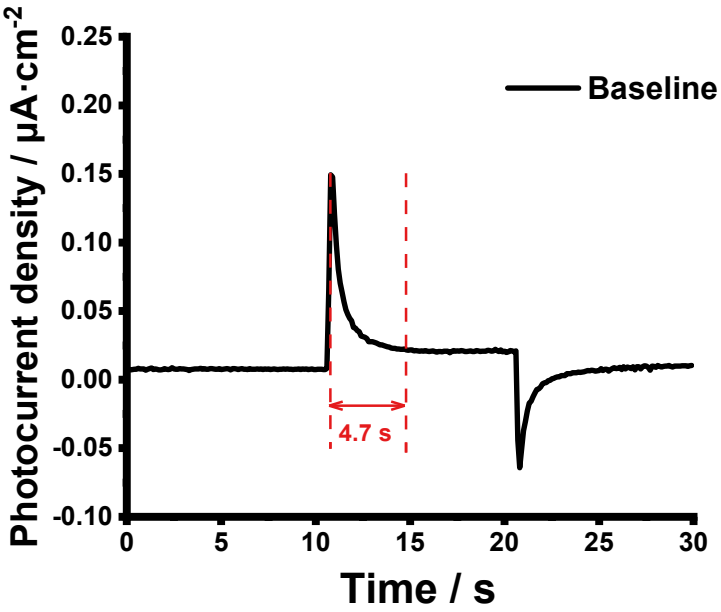

Fig. S32 Time resolution of photoelectrode aptamer/Au SA/TiO_2.

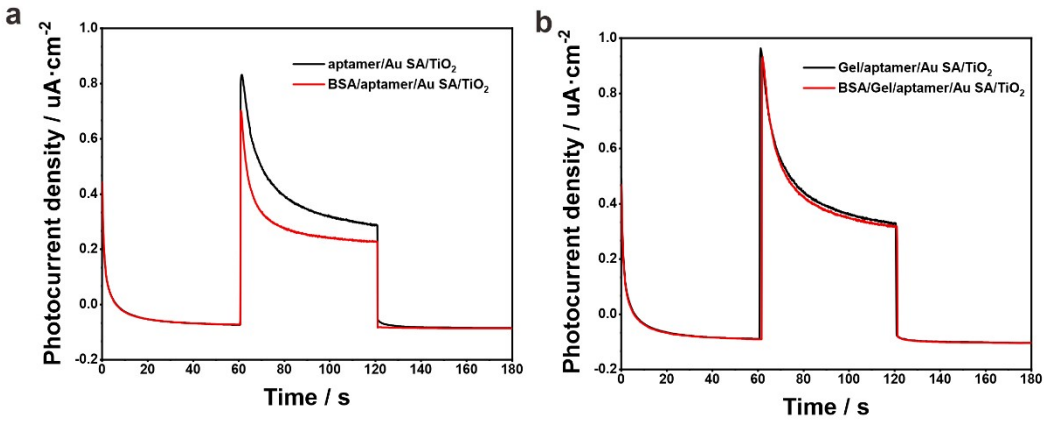

Fig. S33 Photocurrent responses of (a) aptamer/Au SA/TiO_2 and (b) Gel/aptamer/Au SA/TiO_2 electrode after immersing in aCSF containing 20 mg/mL BSA.

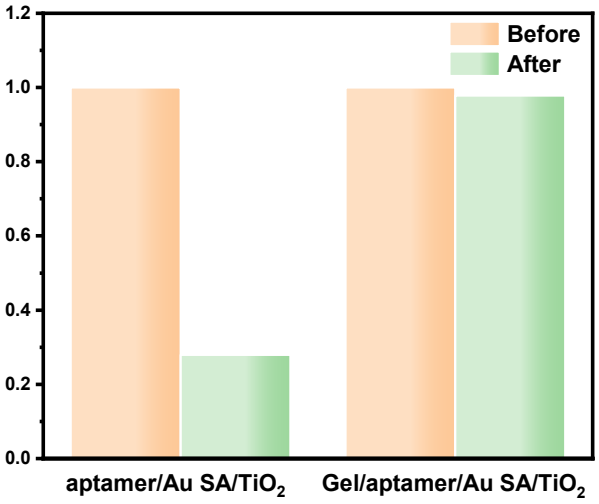

Fig. S34 PEC performances before and after *in vivo* experiment and with/without antifouling layers.

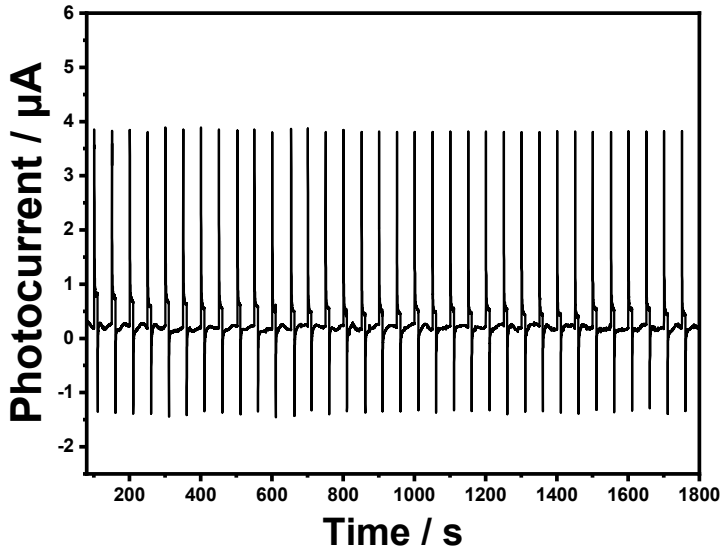

Fig. S35 Representative of photocurrent signal with Gel/aptamer/Au SA/TiO_2 photoelectrode in striatum of mice after injected with saline (0.9%) for 30 minutes.

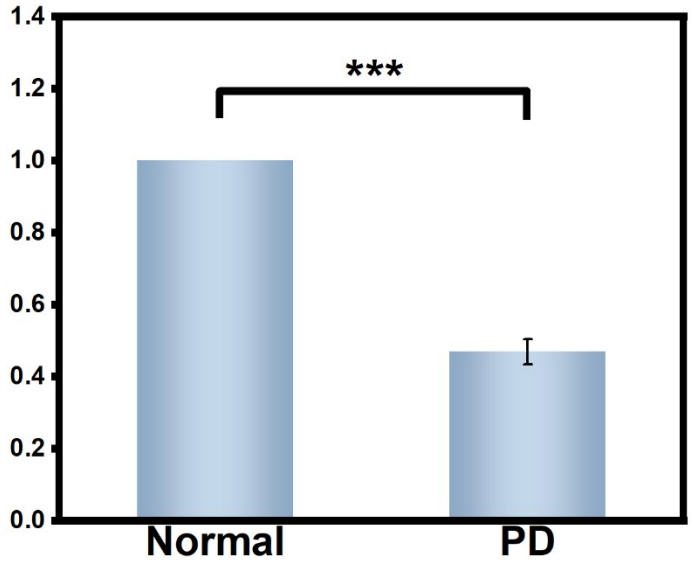

Fig. S36 The comparison of normal and PD anesthetic mice stimulated by injection 80 mM K^+. Data expressed as mean ± SD. Significance was determined by two-tailed unpaired Student's t-test (***$p < 0.001$).

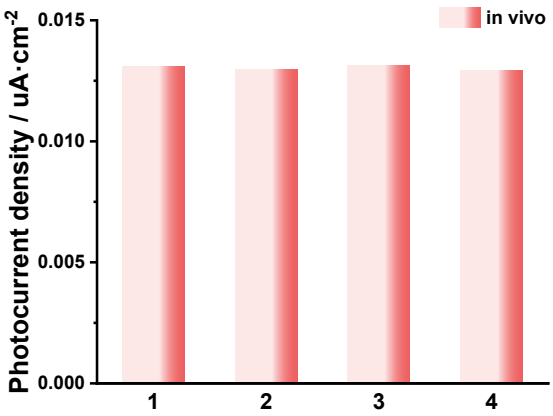

Fig. S37 Photocurrent density of aptamer/Au SA/TiO_2 photoelectrode for *in vivo* analysis in the brain region of Cg (n=4 photoelectrodes).

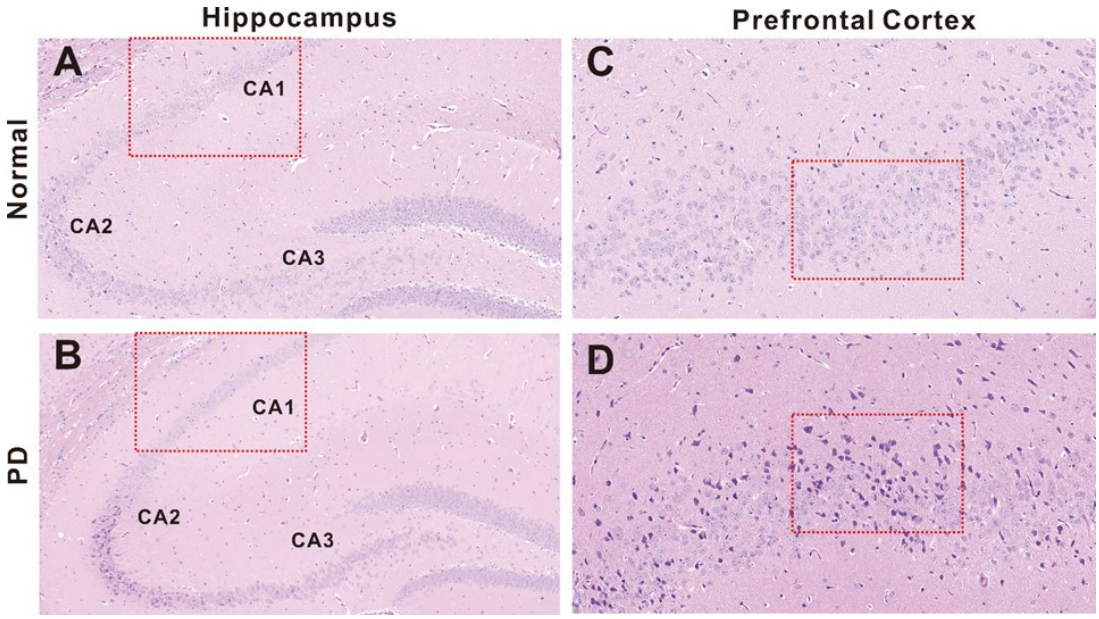

Fig. S38 Hematoxylin-eosin (HE) staining of normal and PD mice in hippocampus and prefrontal cortex.

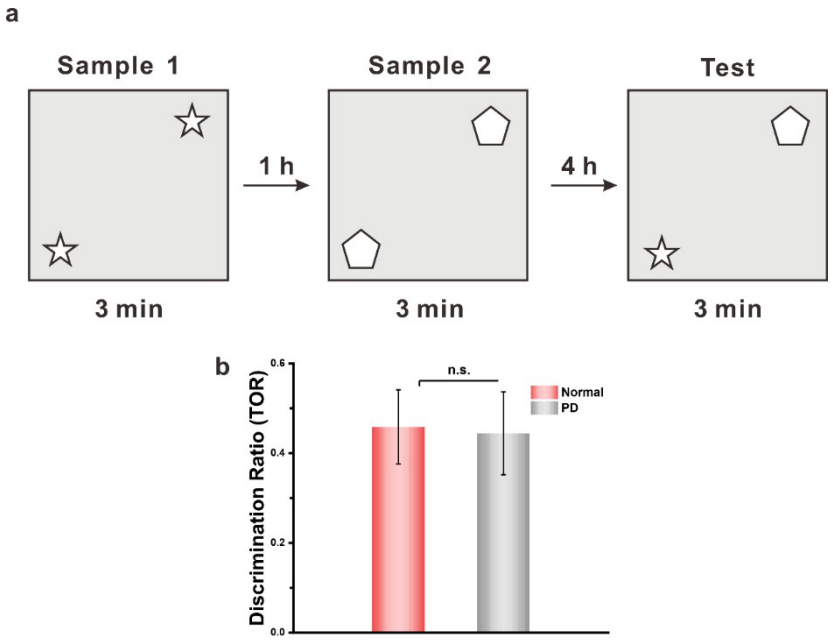

Fig. S39 Schematic illustration of temporal order task (TOR). Data expressed as mean ± SD. Significance was determined by two-tailed unpaired Student's t-test (n.s.>0.05).

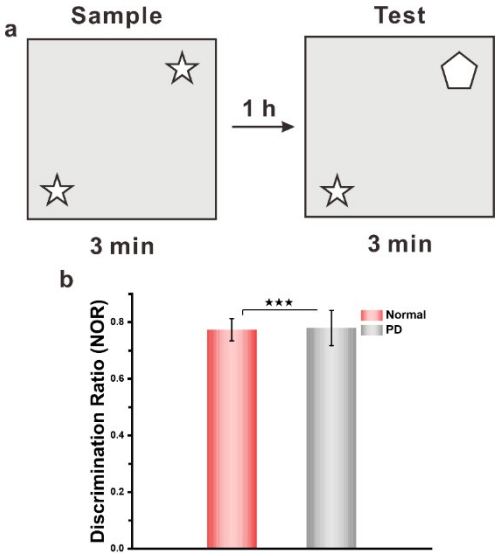

Fig. S40 Schematic illustration of new object recognition (NOR). Data expressed as mean ± SD. Significance was determined by two-tailed unpaired Student's t-test (***p < 0.001).

Table S1. Structural parameters of Au SA/TiO_2 from the EXAFS fitting.

Sample	Path	CN	R(Å)	σ^2(Å^2)	ΔR(Å)	ΔE_0(eV)	R-factor
Au	Au-O	0.5	1.91	0.004	0.071	2.453	0.0098

SA/TiO_2	Au-O	1.6	1.95	0.005	-0.080
	Au-Ti	0.4	2.86	0.003	0.060
	Au-Ti	2.3	3.10	0.020	0.027

S_0^2 is the amplitude reduction factor, which fixed to 0.8. R is the distance between absorber and backscatter atoms; CN is the coordination number; σ^2 is the Debye-Waller factor to account for both thermal and structural disorders; ΔE_0 is the inner potential correction; R-factor indicates the goodness of the fit. Bold value shows coordination number derived from the crystal structures.

Fitting range: $3.0 \leq k$ (Å) ≤ 12 and $1.0 \leq R$ (Å) ≤ 3.1.

Table S2. Comparison of selectivity performance of DA sensors with the interferences of other monoamines.

Biosensor	Selectivity (Response value = monoamines/DA)	Linear range	Limit of detection	Sample	In vivo stability	Reference
aptamer/Au SA/TiO_2	**100 nM NE/100 nM DA = 0.13 100 nM EP/100 nM DA=0.08 100 nM 5-HT/100 nM DA=0.06**	**2 nM-3 uM**	**0.25 nM**	**Mice brain (Striatum, hippocampus, prefrontal cortex)**	**3600 s**	**This work**
aptamer cholesterol amphiphiles	10 uM NE/10 uM DA=0.3	0.5-2 uM	-	Rat brain (Nucleus accumbens and medial forebrain bundle)	Several seconds	Angew. Chem. Int. Ed. 2020, 59, 18996 –19000
COF-modified carbon fiber microelectrode	20 uM NE/20 uM DA=0.1 20 uM EP/20 uM DA=0.13 20 uM 5-HT/20 uM DA=0.06	25 nM-20 uM	8.4 nM	Mice brain (Striatum)	80 minutes	J. Am. Chem. Soc. 2023, 145,23727−23738

$aptCFE_{2.0}$	10 uM DA/10 uM NE=0.09 10 uM DA/10 uM EP=0.21	0.05-20 uM	13 nM	Mice brain (Striatum)	12 hours	Angew. Chem. Int. Ed. 2022, 61, e202208121
PEDOT-PC/CFEs	-	-	-	Rat brain (Striatum)	2 hours	Angew. Chem. 2017, 129,11964–11968
PEDOT/CNT	-	50 nM-500 nM	4 nM	Mice brain (striatum)	4 weeks	Adv. Sci. 2024, 2308212
G-FETs	100 uM NE/100 mM DA=0.08 100 uM 5-HT/100 mM DA=0.06	1 nM-10 uM	10 pM	Mice brain tissue	-	Anal. Chem. 2022, 94, 8605−8617
aptamer/RGO needle FET	1 uM NE/100 nM DA=0.02 1 uM EP/100 nM DA=0.04	1 nM-10 uM	370 pM	Rat brain (Dorsal striatum)	400 senconds	Small 2022, 18, 2204142
DNA, aptamer, Exo III, SG I	30 uM EP/3 uM DA=0.04	0.1-10 nM	0.08 nM	Mice brain tissue	-	Sensors and Actuators B: Chemical, 305, 127348.
Mn-MoS_2/PGS	-	50 pM-5 uM	50 pM in PBS, 5 nM in 10% serum, and 50 nM in sweat	PBS (pH 7.2), artificial sweat, 10% serum	-	Sci. Adv. 2020; 6: eabc4250
$Cu_{2-x}S$@GO-DNA-Au@MoS_2 nanointerface	-	1 aM-1 uM	0.45 aM	Cerebrospinal fluid, whole serum, artificial sweat, DA neuron cells	7000 s	Adv. Mater. 2023, 35, 2304116
Plasmonic biosensor platform	10 mM EP/10 mM DA≈0	-	100 pM (BSA) 90 pM (aCSF)	Protein solutions, aCSF, unprocessed whole blood	-	Sci. Adv.10, eadp7460(2024).

MPC aptamer/SiNW -FET)	10 nM NE/10 nM DA=0.5 10 nM EP/10 nM DA=0.2	0.01 nM-10 nM	0.01 nM	Living PC12 cells	Several seconds	J. Am. Chem. Soc. 2013, 135, 16034−16037
CMC/MIP	-	1 nM-0.1 mM	0.48 nM	-	-	Advanced Functional Materials, 2410546.
Pt/rGO	20 uM 5-HT/20 uM DA=0.05	50 nM-16.3 uM	50 nM	Rat brain (caudate putamen)	~100 seconds	ACS Sens. 2019, 4, 8, 1992–2000

Table S3. Illustration of DA concentration in three brain regions measured by HPLC/FLD.

	Normal	**PD**
Prefrontal cortex	51.18 nM	49.11 nM
Striatum	70.64 nM	20.53 nM
Hippocampus	20.39 nM	18.37 nM